Ultrasonic micromoulding

Gulcur, Mert; Brown, Elaine; Gough, Tim; Romano, Jean-Michel; Penchev, Pavel; Dimov, Stefan; Whiteside, Ben

DOI:
10.1016/j.jmapro.2020.08.033

Document Version
Peer reviewed version

Citation for published version (Harvard):
Gulcur, M, Brown, E, Gough, T, Romano, J-M, Penchev, P, Dimov, S & Whiteside, B 2020, 'Ultrasonic micromoulding: process characterisation using extensive in-line monitoring for micro-scaled products', *Journal of Manufacturing Processes*, vol. 58, pp. 289-301. https://doi.org/10.1016/j.jmapro.2020.08.033

Ultrasonic micromoulding: Process characterisation using extensive in-line monitoring for micro-scaled products

Mert Gülçür (1, *), Elaine Brown (1), Tim Gough (1), Jean-Michel Romano (2), Pavel Penchev (2), Stefan Dimov (2), Ben Whiteside (1)

(1) Centre for Polymer Micro & Nano Technology, Faculty of Engineering and Informatics, University of Bradford, Bradford BD7 1DP, UK

(2) School of Mechanical Engineering, University of Birmingham, Edgbaston, Birmingham B15 2TT, UK

*Corresponding author: Mr. Mert Gulcur, m.gulcur@bradford.ac.uk

Postal address:

University of Bradford
Richmond Rd.
Polymer IRC, EDT 8
Bradford
BD71DP
United Kingdom

All figures should be in colour in the online version.

ABSTRACT

Industry-standard quality management systems such as Six Sigma and emerging Industry 4.0 compliant production processes demonstrate the importance of in-line condition monitoring of manufacturing methods for achieving the highest levels of product quality. Measurement data collected as the process is running can inform the operator about unexpected changes in machine operation or raw materials that could negatively impact production; and offer an opportunity for a process control intervention to stabilise production. However, micro-manufacturing production lines can pose a challenging environment for deploying such systems, since processing events can occur extremely rapidly and in harsh environments. Moreover, the small scale of micro-nano featured components can make sensor installation even more problematic.

Recently, ultrasonic micromoulding has drawn attention in niche markets due to its unique advantages for processing thermoplastics as a new micro-manufacturing technology. The process differs from conventional moulding significantly by eliminating the need for a plasticising screw and using direct application of ultrasonic energy to melt the polymer. This offers numerous benefits such as decrease in energy usage, moulding at lower pressures, easier cleaning, and reduced material residence times, the latter which could be beneficial for pharma-grade polymers or polymers with active ingredients. However, very little work has been reported attempting to monitor the process using in-line measurements. This work aims to evaluate the characteristics of the ultrasonic micromoulding process for microinjection moulding of a microneedle array using a range of sensor technologies including: data recorded by the machine controller; a high-speed thermal camera and a cavity pressure transducer. The data has captured the highly dynamic process environment with a high degree of accuracy. The relationship between the process data and dimensional quality of the ultrasonically

micromoulded products has been quantified and subsequently implemented as a cost-effective in-line quality assurance method.

Keywords: ultrasonic micromoulding, micro-injection moulding, process monitoring, data acquisition, polymer replication, microneedles.

HIGHLIGHTS

- Each stage of the ultrasonic micromoulding process have been characterised
- The highest melt temperatures have been recorded after the cavity filling
- As-supplied machine data have been proved to be a very useful source for in-line monitoring of ultrasonic micromoulding process
- A cost-effective method for quality assurance of microneedles has been demonstrated.

1. Introduction

Micro-injection moulding or micromoulding technology has evolved into an established and highly-repeatable manufacturing process over the last two decades for producing miniature products with intricate features and micro-nano textured surfaces [1-6]. Despite this, some inherent aspects of this technique can prove problematic for certain applications. For instance, the use of extruder screws for plastication means that there is a particular volume of molten material within the machine required to run the process. This can cause long residence times and pose problems when processing pharmaceutical grade polymers, which are typically less stable at high temperatures than their engineering polymer equivalents [7, 8]. Material wastage can also be a significant issue as the sprue and runner systems of the products can form up to 97% of the total shot amount while moulding small components [9, 10]. In an attempt to address some of these challenges, new concepts for plasticising and micromoulding of polymers using ultrasonic energy have emerged [11-13].

The ultrasonic micromoulding process has been dubbed as an alternative and viable option for manufacturing miniature products from thermoplastics where ultrasonic energy is utilised to plasticise the feedstock [9, 14]. The process offers significant benefits over conventional micro-injection moulding techniques including energy efficiency, material savings and very short residence times [15, 16]. Ultrasonic micromoulding uses simultaneous melting and injection of the polymer by means of sonication, allowing the polymer to be exposed to high temperatures for only a few seconds. This is significantly different to conventional micromoulding processes where the polymer is plasticised using a screw-barrel system and the molten material remains at elevated temperatures in the barrel for some time – typically a minimum of ten minutes, increasing to several hours in some cases. The much shorter residence times for ultrasonic micromoulding can be very beneficial for processing of pharmaceutical polymers where degradation could be an important issue [9].

The interest and number of research papers for ultrasonic moulding or micromoulding of polymers has been increasing in recent years due to the aforementioned potential [9]. A variety of polymers including polypropylene (PP), polylactide (PLA) and polyetheretherketone (PEEK) have been used for ultrasonic micromoulding of small parts by different authors in the literature [16-18]. Zeng et al. carried out work on ultrasonic micromoulding of PP by studying the filling behaviour, effect of processing conditions, mechanical properties and crystallisation behaviour of moulded samples [16]. Higher degrees of crystallinity in ultrasonically moulded samples compared with conventional moulding were reported by the authors. Chemical, mechanical and microstructural properties of ultrasonically moulded polylactide parts have been studied by Sacristán et al. [17]. The authors were able to set process conditions which resulted in samples having similar molecular weight characteristics to the feedstock suggesting minimal degradation of PLA parts moulded using an ultrasonic micromoulding apparatus. Dorf and co-workers optimised the process parameters for producing PEEK tensile bars using a state-of-the-art ultrasonic micromoulding machine [18]. The work focussed on optimising process conditions for obtaining a completely filled tensile bar shaped part and the study of its mechanical properties. One of the main outcomes of this work is that the mechanical properties of the ultrasonically micromoulded samples were comparable to samples moulded with conventional injection moulding. This suggests that ultrasonic micromoulding can be a viable alternative to conventional techniques for low or medium volume manufacturing for specialised applications. However, the work lacked process condition monitoring aspects and repeatability assessment. As can be seen from these studies, most work has focused on optimising a process window for specific materials and their resultant material properties rather than characterising the dynamics of the ultrasonic micromoulding process environment.

A limited research and process insights are available in the literature regarding in-line process monitoring of ultrasonic micromoulding [13, 19-21]. One of the first reports on the matter

presents the monitoring of the sonotrode position and generator power throughout the process [13]. In the work, Michaeli et al. identified compression, melting, and holding phases of the ultrasonic micromoulding process through interpretation of sonotrode position data. However, the in-depth analysis of these process outputs for consecutive cycles is not presented. Heating mechanisms of polymers during sonication have also been studied using a temperature sensor for monitoring purposes at the interface of the feedstock and through use of computer modelling [19, 22]. Only two of the recent reports available present in-line thermal imaging of polymer melts and direct temperature readings from the process [20, 21]. These two reports show that the temperature distribution of the polymer melt is very different from conventional micromoulding where the highest temperature values are observed following the complete filling of the micromoulding cavities. However, these reports do not combine temperature measurements with other condition monitoring techniques. Moreover, it needs to be stated that only these two reports use a state-of-the-art ultrasonic micromoulding machine (Sonorus 1G – Ultrasion SL); the only commercial machinery available for this technology. This is important from a manufacturing point of view as the repeatability of a moulding process is crucial if this new technology is to be considered as an alternative way of producing micro-nano featured parts. Hence, monitoring, and detailed characterisation of a state-of-the-art ultrasonic micromoulding machine is necessary for understanding the process dynamics and providing a complete evaluation of this technology from a micro-manufacturing perspective.

This work aims to provide essential information for understanding the fundamentals of the ultrasonic micromoulding process through the implementation of several sensor technologies including machine data, thermal imaging, and cavity pressure measurements. The interrogation of the collected process data will also shed light towards tackling the fundamental issues of ultrasonic micromoulding such as material dosage, obtaining a homogenous polymer melt and longer cycle times due to higher mould temperatures. Moreover, by characterising the main

stages and features of the process, this new manufacturing technology can be taken to the next level where automation and real industrial applications can be considered.

2. The ultrasonic micromoulding process

2.1 Ultrasonic plasticisation for micromoulding

The hardware used in this work was a Sonorus 1G ultrasonic micromoulding machine with a mould tool for producing thermoplastic microneedle arrays. The machine has a vertical configuration and the melting process is carried out by compressing the polymer feedstock against the ultrasonically vibrating sonotrode using an injection plunger with a diameter of 8 mm (Fig. 1).

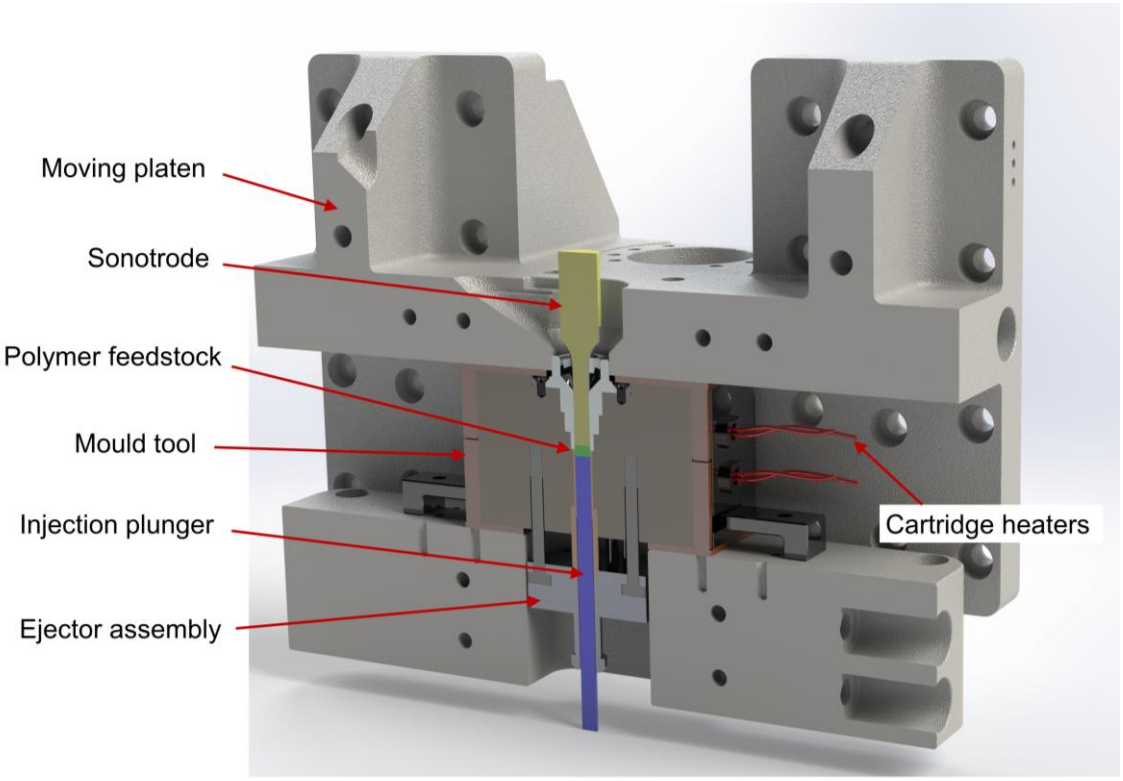

Fig. 1. Schematic showing the main features of Sonorus 1G ultrasonic micromoulding machine.

In the default configuration of the machine, the dosing of the material is performed using a laser-based pellet counting apparatus rather than a mass or volume measurement of the feedstock. The usage of a pellet counting system introduces additional variability in the process as the standard pellet size or mass used in polymer industry varies from particle to particle as well as between different materials. In our previous work, a standard deviation of 5.3 mg was reported out of 18 cycles with an average shot size of 237.6 mg for polypropylene (PP) pellets which is a significant barrier to process repeatability [23]. Moreover, the contact points of the polymer feedstock and variability in the total surface area between the pellets are likely to have impact on interfacial friction and heating that can lead to inconsistencies in part quality [22]. For that reason, instead of pellets, disc shaped preforms have been used in this work to eliminate the variability that could arise from the feedstock shape as shown in Fig. 2a. In the figure, the disc shaped feedstock being placed on the injection plunger without any voids between the discs. The plasticisation of the feedstock is initiated after the material makes its contact with the sonotrode which vibrates at 30 kHz (Fig. 2b). Interfacial friction between the pellets or discs acts as an initiator of the melting process [22]. Then, the heat dissipation is dominated by the damping of the oscillations within the molecular chains of the polymer due to its viscoelastic behaviour [19]. As a result, a significant drop in viscosity is achieved and, through the movement of the injection plunger position, the material is simultaneously conveyed or injected while being plasticised and the melt flow front progresses towards the gate and the mould cavity. It is usually necessary to sonicate the feedstock until the mould cavity is completely filled as shown in Fig. 2c. This is because the polymer melt tends to solidify rapidly once it enters the colder mould cavity. Furthermore, this post-filling sonication is beneficial for replication of micro and nano features since the heat energy is constantly being provided by the sonicating horn in the form of viscoelastic heating and interfacial frictional heating between the melt/mould cavity interface.

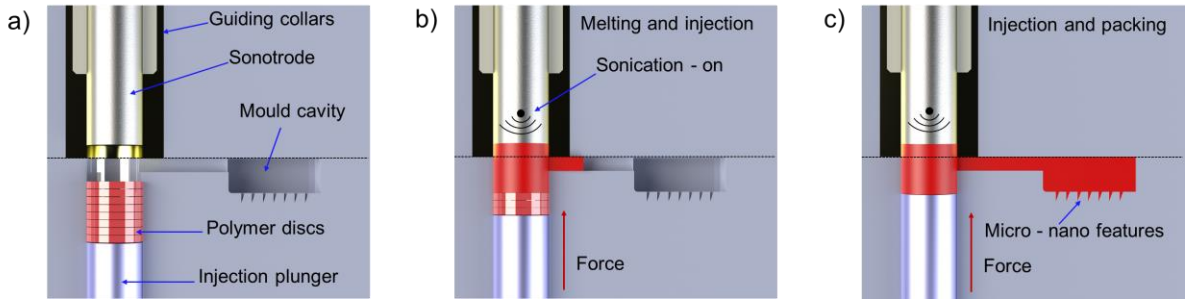

Fig. 2. Schematic diagrams depicting different stages of ultrasonic micromoulding process: a) Polymer feedstock is placed in the sonication chamber, just above the injection plunger; b) feedstock is compressed against the vibrating sonotrode; c) feedstock is melted and the mould cavity with micro-nano features is replicated. The representative geometry of the part is not to scale.

2.2 Tool design for ultrasonic micromoulding

A mould tool with a straight runner and a circular mould cavity has been designed and manufactured for ultrasonic micromoulding monitoring purposes (Fig. 3.). The main circular base of the part has a diameter of 17.5 mm, which can hold flush-mounted mould inserts with a diameter of 10 mm as depicted in Fig. 3a and b.

A laser machined microneedle mould insert was used in this study. Microneedle cavities on the mould insert were arranged in a 6x6 configuration and each conical microneedle cavity has circa 940 µm of depth, 630 µm base and 3-5 µm of tip radius. A laser source (Satsuma model - Amplitude Laser), with 310 fs pulse duration, 1030 nm wavelength, maximum average power of 5 W and maximum pulse repetition rate of 500 kHz was used for machining the cavities. The laser processing parameters can be seen from Table 1. A beam spot diameter of 30 µm was steered over the focal plane using a 3D scan head (RhoThor RTA – Newson), equipped with a 100 mm-focal length telecentric lens. A hatch distance of 4 µm was used in a x-y raster scanning mode on the insert surface with 45° rotation of the laser hatching direction in each

layer which results in a better surface quality. The slice thickness (the step height along Z axis), which corresponds to the ablation rate per layer was 1 μm and it was executed with the Z-module of 3D scanheads in order to benefit from its high dynamics capabilities in comparison to the ones of the mechanical stages. A circular laser beam polarization was used in order to achieve sharper and deeper microneedle cavities without residual directionality on the insert surface plane, which are existent when using a linear beam polarization. Preliminary trials allowed identifying the laser machining parameters that removed a homogeneous layer of 1 μm depth (see Table 1). Cavities were then machined by implementing a layer-by-layer approach until the targeted depth was achieved (Fig. 3c). Generation of the toolpath for the laser machining trials was performed with commercially available CAD/CAM software (Autodesk ArtCAM) with a custom built postprocessor [24]. The resultant laser machined cavities were designed to be in a double-tapered structure which makes the filling process particularly challenging towards the bottom of the microneedle cavity (Fig. 3c).

Table 1. Laser machining parameters used for creating microneedle cavities.

Parameter	Value & units
Laser power	3.5 W
Laser repetition rate	500 kHz
Scanning speed	2000 mm/s
Scanning hatch distance	4 μm
Ablation rate per layer	1 μm

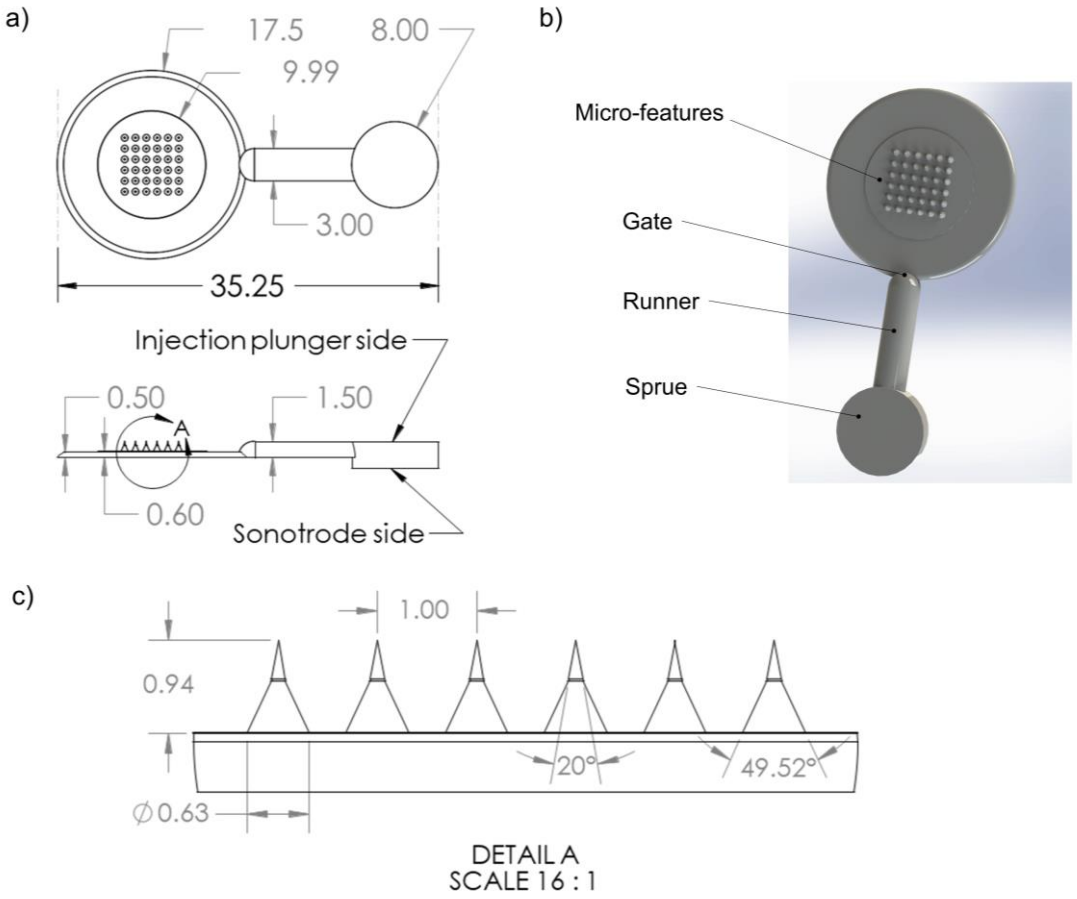

Fig. 3. Ultrasonic micromoulding part design details: a) Dimensions of the part in mm; b) 3D rendered image of the part showing important features; c) cross-section and dimensions of the microneedle features. Double-tapered structures of the needles are also indicated with angles.

Flow visualisation has been a powerful method for studying flow behaviour, shrinkage, internal stresses and cooling behaviour of polymer melts in micromoulding research [2, 21, 26, 27]. In order to carry out thermo-optical visualisation of the polymer flow during the filling stage of ultrasonic micromoulding, a sapphire window has been flush-mounted on the top mould (Fig. 4). Sapphire is transparent in the infrared spectrum for wavelengths below 6 μm, hence, this arrangement allows the melt temperature values to be recorded directly during the ultrasonic micromoulding process.

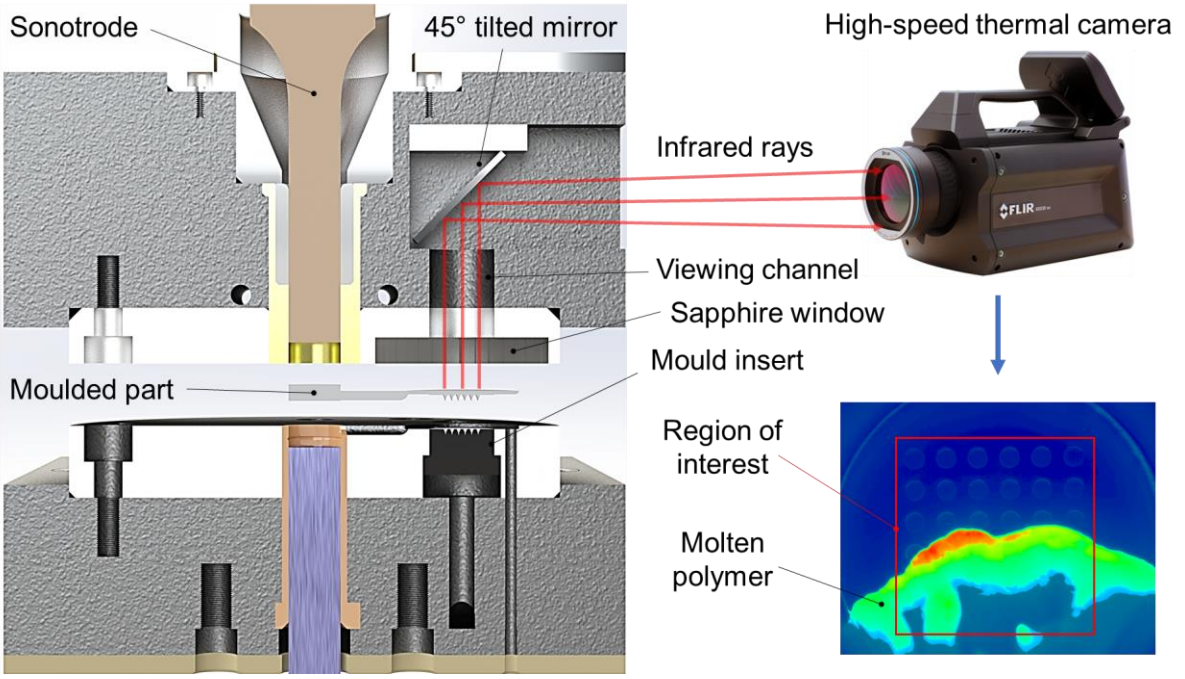

Fig. 4. Flow visualisation mould tool for ultrasonic micromoulding and details of the optical train including a thermal image of the molten polymer progressing through the cavity.

2.3 Materials

A generic injection moulding grade polypropylene resin (Ineos - GA12) was used in this work. PP provides a well-defined starting point for process monitoring purposes since it is a relatively easy material to process due to its good flowability [25]. Some of the important physical properties of this PP are given in Table 2.

Table 2. Physical properties of Ineos 100-GA12 PP resin.

Properties	Value & units
Melt flow rate at 230°C/2.16 kg	12 g/10 min
Tensile strength at yield	34 MPa
Heat deflection temperature at 0.45 MPa	90°C
Shrinkage [25]	1 - 2.5 %
Density	0.895 - 0.92 g/cm³

In order to characterise the ultrasonic micromoulding process accurately, the inherent issues related to the variability in shot size and amount of total surface area of the feedstock had to be eliminated. This has been achieved by using injection moulded PP disc shaped preforms instead of industry standard pellets. The discs have a diameter of 8 mm and can be placed just above the injection plunger without any voids that could cause variability during the process. The plunger and the sonotrode also have an 8 mm diameter and the flat surfaces of the discs provides a homogenous first contact with the ultrasonic horn when the sonication starts. The thickness of the discs was set as 1.5 mm and four discs were used to create a shot weight of 260 mg with a standard deviation of 0.58 mg from 18 measurements.

The semi-crystallinity of PP is characterised by its sharp melting point at circa 165°C as can be seen from the differential scanning calorimetry (DSC) results presented in Fig. 5. Three measurements for each shape of feedstock were carried out. The melting point of PP discs was measured to be ~1.208°C lower than the virgin material, which confirms that no significant difference is present between the disc preforms and pellets that could arise from the thermal history of the material.

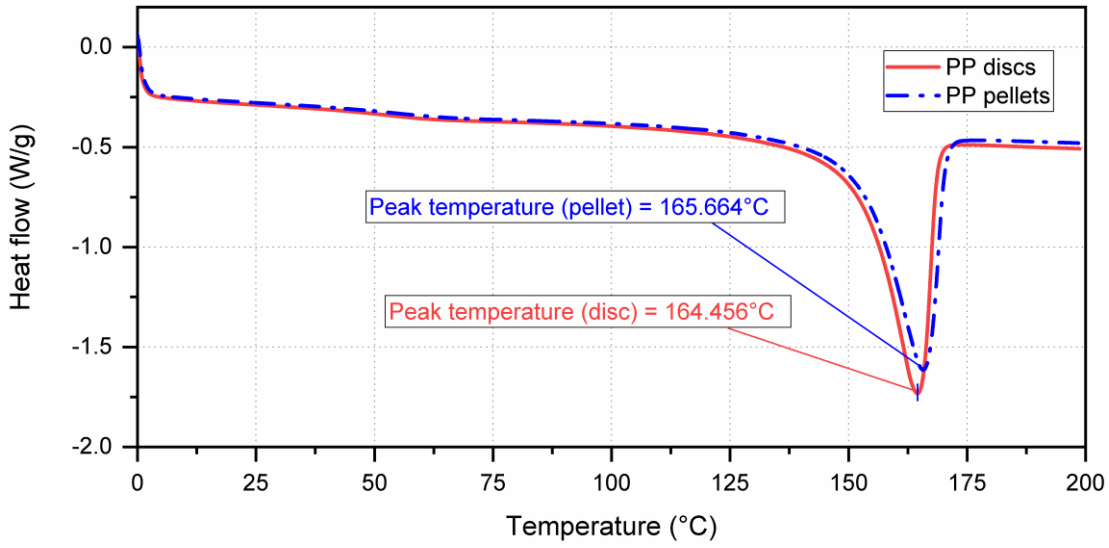

Fig. 5. DSC tests for PP pellets and discs indicating the melting points for each form of material.

2.4 Process settings and moulding of parts

The process parameter optimisation for ultrasonic micromoulding for a range of thermoplastic materials has been studied by different groups and reported in the literature [17, 28-30]. The Sonorus 1G machine has a highly-flexible multi-stage profiling capability for process optimisation, however for simplicity and to reduce the number of unknowns, the parameters were kept constant throughout the process. The sonication amplitude (A_{sonic}) is the peak to peak displacement of the sonication horn and can be applied up to 96 μm. The heat energy generated per unit time during plasticisation of feedstock has a square dependence to A_{sonic}, and this parameter stands out as one of the most important variables that is decisive in the melting of the feedstock [19]. The semi-crystalline polymers require higher amplitudes than amorphous materials for overcoming the latent heat due to their relatively ordered structure and the maximum available amplitude of 96 μm was used for ultrasonic micromoulding of PP. The sonication duration (t_s) is another important parameter to consider, where the total sonication or heat energy given to the system during melting, injection and packing stages is defined by this parameter in conjunction with the power consumption of the sonicating horn. 4 s of sonication time was sufficient for achieving a complete part and good packing in the experiments. The melting of the polymer and the injection of the molten material towards the micromoulding cavity is facilitated by compressing the polymer feedstock against the vibrating sonotrode with an injection plunger as indicated in Fig. 1. This compression force is termed as the injection force (F_i) during the ultrasonic micromoulding process. F_i has to be selected carefully and be as low as possible since loading the sonotrode with excessive forces will lead to an increase in the resonant frequency of the horn leading to overloading of the signal generator. 750 N injection force was used for obtaining completely moulded parts. This force corresponds to an injection pressure value of 149.3 bar which is significantly lower than the pressures used in conventional micromoulding for comparable part geometries [31].

Mould temperature (T_m) is an important parameter for achieving successful micro-nano replication of the mould features in conventional micromoulding, ultrasonic micromoulding and hot embossing [1, 2, 10, 32]. The parameter is of great importance in ultrasonic micromoulding since, due to the machine design, it is inherently impossible to apply higher injection forces (typically $F_i > 2000$ N) in order to prevent the premature solidification of the molten polymer while it travels towards the mould cavity. This is due to the presence of an elastic belt, which connects the ultrasonic stack to the servo motor. The belt elastically deforms as excessive forces are applied leading to changes in default sonotrode position during melting which should be prevented. Thus, ultrasonic micromoulding usually requires slightly higher mould temperatures than conventional micromoulding processes to ease the injection stage of the process and avoid sonotrode overloads. A mould temperature of 90°C, towards the highest values that can be applied for this particular material, was used for replicating the deep microneedle features.

The current state of the machine lacks a closed-loop feedback control for pressure controlled switchover and each stage of the filling is defined and controlled by the piston position. Moreover, sonication time also defines the length of a full moulding cycle including melting, injection, and filling process. For maintaining a relatively repeatable process, a procedure has been adopted where the cavities are part filled for given filling forces and the sonication kept on for a few seconds that facilitates the complete filling and replication of micro-nano features on the moulds. These sonication times during packing should be kept as short as possible (~1 s) for preventing the overloading of the sonotrode. Although this procedure allows us to mimic a switch-over that is being carried out in state-of-the-art micromoulding machines, it is very difficult to provide a well-defined point where prolonged sonication is harnessed for packing as inconsistencies are present in the melting due to feedstock shapes and melt inhomogeneities.

In order to be able to record the most relevant process data, 10 parts were initially moulded and discarded for stabilising temperature gradients on the parts of the machine. 15 samples were then consecutively moulded and collected back to back to mimic a production cycle. The process settings used for experimentation are given in Table 3 and were kept constant for all parts.

Table 3. Ultrasonic micromoulding parameters used for PP.

Parameter	Value & units
Sonication amplitude (A_s)	~96 μm
Sonication duration (t_s)	4 s
Injection force (F_i)	750 N
Mould temperature (T_m)	90°C
Cooling time	10 s

2.5. Ultrasonic micromoulding process monitoring

Process data measurements were carried out using three main sources:

(i) Machine data – this comprises the encoder position of the injection plunger, sonication frequency of the sonotrode, injection force and ultrasonic generator power channels

(ii) Thermal imaging – a high-speed infrared camera captures the flow of the molten polymer into the mould cavity through a sapphire window allowing temperature values to be extracted directly from the micromoulding cavity

(iii) Cavity pressure measurements – an indirect cavity pressure transducer has been installed at the back of one of the ejector pins which is located at the end of the circular mould cavity.

Machine data have been collected using the ethernet connectivity of the Sonorus 1G at a 100 Hz data acquisition rate. The source for measuring the sonication frequency and the power measurements is the analog output of the ultrasonic signal generator (Branson 50DCXs30VRT). Injection force and plunger position are calculated internally by the machine software via reading the servomotor torque and revolutions, respectively. Thermal imaging acquisitions were carried out using a high-speed thermal camera (FLIR X6540sc) at 100 frames/s with 50 μs integration time that is capable of measuring the temperature range of 128.1 – 266.5°C. The temperature values exceeding this limit are extrapolated by the thermal camera software. A 640 x 512 pixels window corresponding to a 90 x 70 mm^2 area which visualises the majority of the circular cavity was set for thermal images. A typical emissivity value of 0.97 for PP has been set. Cavity pressure measurements were performed using a Kistler 9210AA miniature indirect sensor, which is connected to Dynisco CHA 4020 amplifier. The amplifier output was then connected to a National Instruments NI-9215 module and cDAQ –

9185 ethernet chassis for recording the data at 100 Hz. All three sources of measurements have been synchronised with a 5 V trigger signal taken from the ultrasonic generator which becomes active when the sonication starts.

3. Results and discussion

3.1 Machine data measurements

Typical machine data captured from a single ultrasonic micromoulding cycle with the aforementioned tooling configuration are shown in Fig. 6. The particular region of interest in the graph is the sonication stage (t = 0 - 4 s) where the compression of the feedstock, melting and filling phases are being carried out. Dramatic changes in power output (blue curve) and sonication frequency (green curve) were observed and this is due to the load acting on the sonotrode because of the compression of the feedstock which becomes molten after t = 1 s. Between t = 0 - 4 s, the injection plunger applies F_i set by the user (750 N) and the force reduces to 500 N after t = 4 s when the machine enters the cooling and packing phase. This default force does not have an impact on the filling behaviour although slight displacements in plunger position are seen towards -2 mm. Flashing effects are observed around the sprue of the part in cycles where these displacements are significant during the cooling and packing phase. The purpose of the default force is to keep the structural integrity of the sprue which is beneficial for ejection of the part after the moulding process is complete. Overall, the data indicate that it is sensible to take the plunger position information as a datum when characterising different stages of the ultrasonic micromoulding process since each of the phases - compression, melting and filling can be traced easily from this measurement

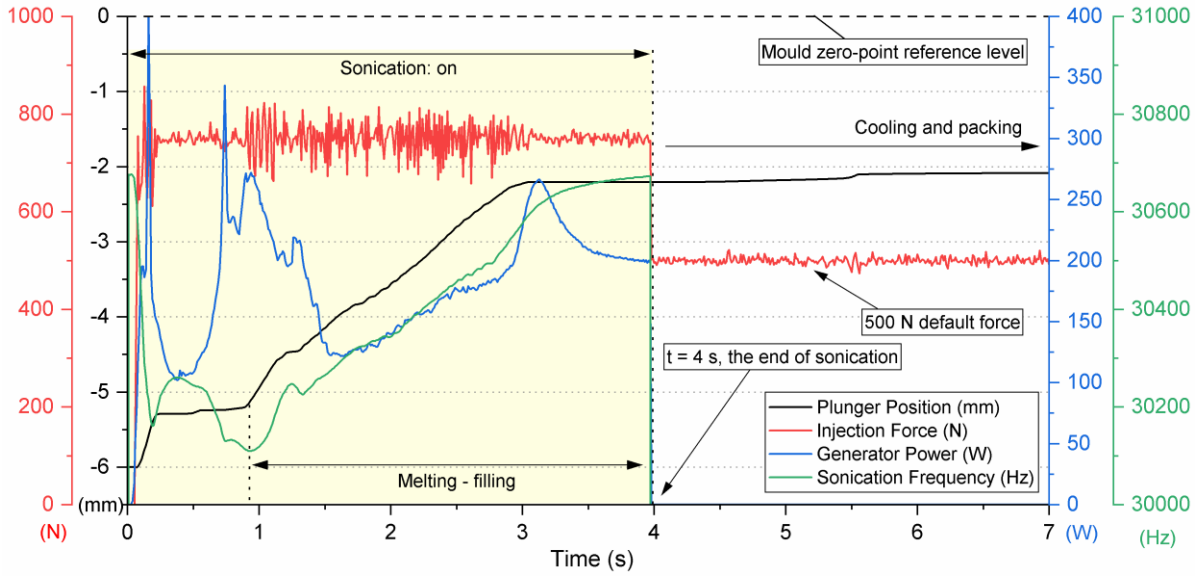

Fig. 6. Machine data captured during ultrasonic micromoulding of PP from the 1st cycle.

Plunger position data generated from three consecutive moulding events are shown in Fig. 7. The data show the free movement of the plunger until the feedstock makes the first contact with the sonotrode between t = 0 – 0.25 s. Following the first contact, a plateau is present where the elastic compression of the discs against the vibrating sonotrode occurs. At this stage, the frictional heating between the surfaces of each disc act as initiators of the melting process and the material starts to flow at approximately t = 0.8 s. It can be seen from the data that the position data can vary significantly from cycle to cycle. This is clear from the points where the feedstock starts to melt at t = 0.75 s for the 11th cycle (blue curve) and at t = 0.9 s for 10th cycle (green curve). This behaviour is expected since, although the surface roughnesses of the disc shaped preforms and initial contacts are the same, the amount of interfacial friction can still be affected since the preforms are placed manually in the sonication chamber. The curvature for plunger position during melting and injection phases for all three cycles are similar, albeit some deviations are present. This can be attributed to the semi-crystalline nature and abrupt melting point of PP which can cause partial melting in different regions of the feedstock.

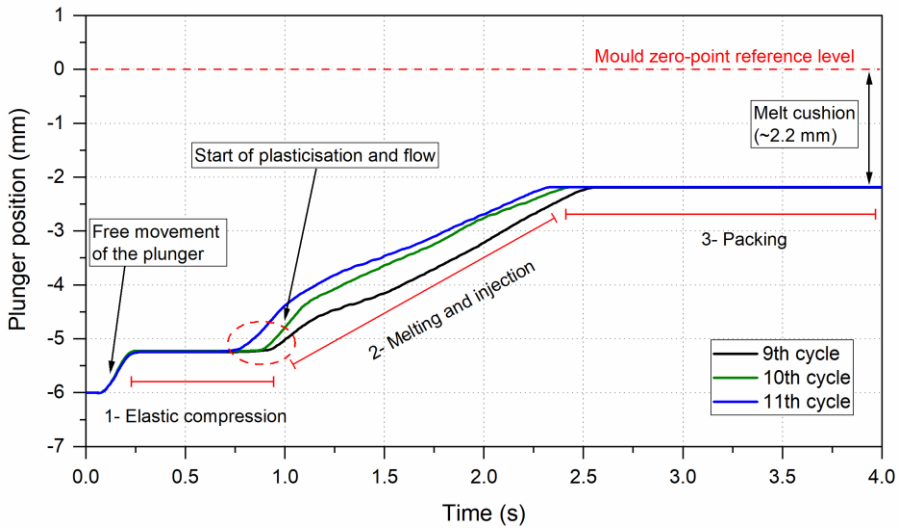

Fig. 7. Plunger position recorded from three consecutive ultrasonic micromoulding cycles while the sonication was applied.

The monitoring of sonication frequency and power drawn by the signal generator are also of interest for maintaining a stable and repeatable melting and injection. If the sonotrode is overloaded by excessive loads, the machine ceases its operation and the moulding process is interrupted. A detailed description of the sonication phase of the process including power and sonication frequency curves is shown in Fig. 8. The figure illustrates five points of interest during the moulding process:

(1) Start of contact: the sonication frequency decreases between t = 0 s to t = 0.2 s until contact is first made with the disc preforms. Between t = 0 – 0.2 s, the sonotrode vibrates freely without any force acting on the horn, hence a decrease towards 30 kHz which is the resonant frequency of the ultrasonic stack is observed. This has been verified by the power data with a sharp peak near t = 0.2 s occurring where the transducer draws the maximum current as the frequency shifts to the resonance conditions. The data also show a sharp increase in sonication frequency when the sonotrode makes the first contact with the polymer discs at t = 0.25 s. This can be explained by the fact that any load that could shorten the length of the ultrasonic stack (even in micro-scale) will result in an increase for the resonant frequency of the horn. The power drawn also decreases significantly once the sonotrode is out of phase with the signal coming from the ultrasonic signal generator.

(2) Elastic compression: the sonotrode is under load by the force applied via the plunger and a slight increase in frequency near t = 0.4 s can be observed. One could expect the sonication frequency to increase continuously under loaded conditions, however, starting from t = 0.6 s the polymer discs start to plasticise and a slight decrease and a local minimum can be seen near t = 0.9 s.

(3) Start of flow: at this point the polymer starts to flow and is conveyed towards the runner. Power draw also increases due to the change in sonication frequency which decreases towards 30 kHz.

(4) Melting and injection: the sonotrode is constantly under load by the compression of the feedstock which is being plasticised and sonication frequency increases steadily.

(5) Packing: the plasticised material can no longer be conveyed since the cavity is completely filled. This can also be identified from the increase in sonication frequency because of the increased load as the molten material is now being packed instead of being injected and conveyed freely. The duration of sonication in the packing phase is very important as the frequency continues to increase with applied force and it is highly likely that the sonotrode will be overloaded with excessive sonication durations.

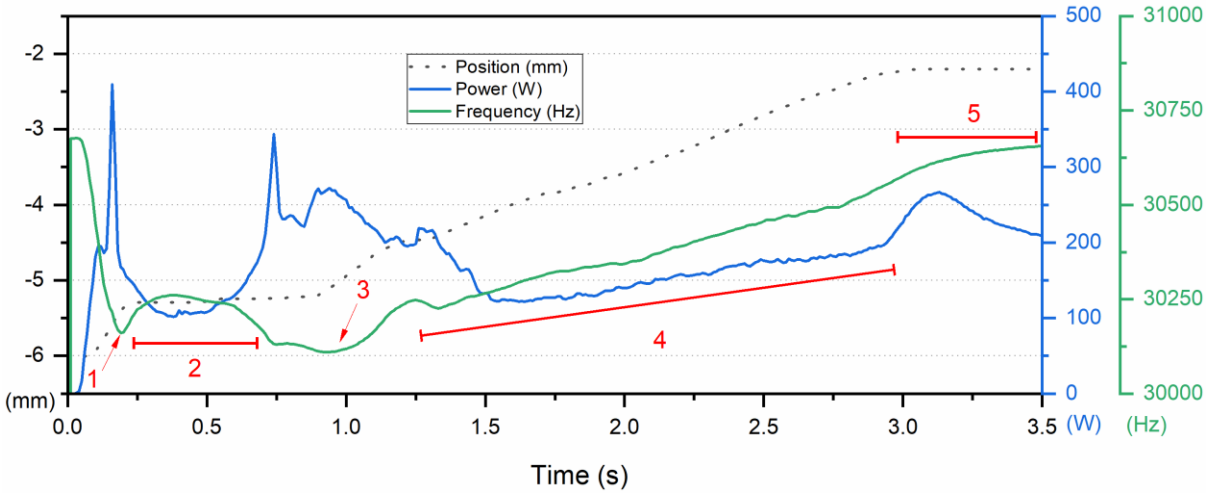

Fig. 8. Sonication frequency and power output captured during the 1st cycle. Important features and regions are numbered and discussed in detail in the text.

These data taken from the machine sensors show that they are essential for understanding the compaction, melting, injection, and packing phases of an ultrasonic micromoulding cycle. The plunger position stands out as one of the most important data channels since different stages of the process can be traced easily by analysing this curve in detail. The data is also useful when the sonication frequency and power consumption during the sonication process are being interrogated. It was also seen that each channel of machine data could change significantly from cycle to cycle, however, the main features of the process plots were repeated for all manufactured parts.

3.2 Thermal imaging acquisitions

Flow visualisation using high-speed thermal imaging has been shown to be an extremely powerful technique to measure the temperature of polymer melts during conventional micromoulding processes [2, 21, 23, 27, 33, 34]. The viscosity of the polymer melt is directly proportional to the measured temperature during the flow which can be correlated to the micro or nano replication quality [27, 35]. The technique is of critical importance for ultrasonic micromoulding as there is no direct ability to set the melt temperature during sonication. Instead, the temperature is determined by the energy transfer from the sonotrode during excitation and the extent of heat losses through the mould. Thermal imaging can view these outcomes directly and allows immediate quantifications of actual melt temperatures and uniformity of heating of the melt during cavity filling.

The simultaneous melting and flow of PP during ultrasonic micromoulding are complex processes because of PP's inherent semi-crystallinity. The crystallites within PP absorb the high frequency mechanical vibrations and the energy required for overcoming the heat of fusion could change locally when the contact points of the feedstock are considered. This results in partial and complete melting of the polymer discs in randomised local areas leading

to an inhomogeneous temperature and viscosity distribution during the process. The flow of PP in ultrasonic micromoulding is usually characterised by an initially asymmetric flow front and unequal temperature distributions in the melt until the end of the filling process as can be seen from the thermal images in Fig. 9. Moreover, it has been known that ultrasonic waves propagate significantly different in solids and polymer melts [36]. From that perspective, the regions that melt first and propagate locally with reduced ultrasonic attenuation improve the flow, causing a further reduction in viscosity. Towards the end of the process (t = 2.6 s and t = 3.36 s), a hotter region near the gate can be seen as a result of the sonication provided by the horn until t = 4 s. This is an interesting feature of ultrasonic micromoulding since sustaining this sonication energy results in higher temperatures in the polymer melt towards the end of the filling process.

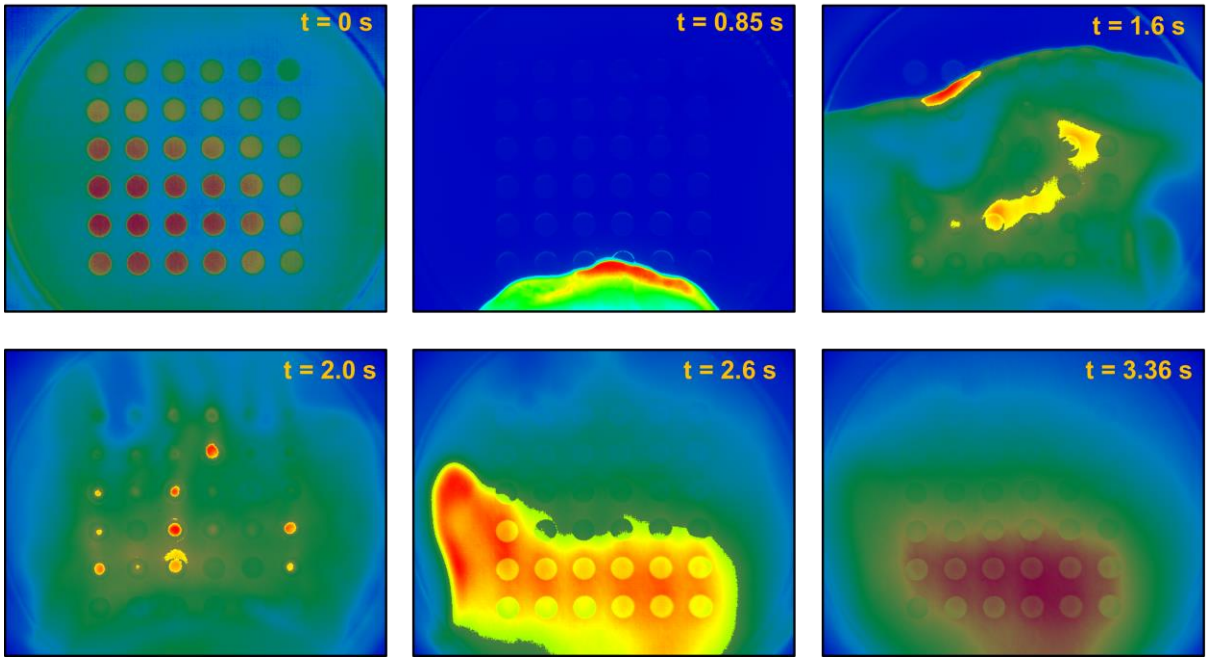

Fig. 9. Thermal images taken from the filling event of 13th cycle. A variable scale is used in each image to show the unequal temperature distributions.

The highest melt temperatures that are occurring after the filling were confirmed by extracting the mean temperature values from a square region of interest that covers the microneedle features. Fig. 10 shows the temperature recordings taken during 13th cycle alongside the injection plunger position data. The features of interest can be discussed in detail as following:

(1) The start of the flow or the injection phase have been verified by the point where the increase in plunger position is accompanied by the temperature increase. It should be noted that the temperatures recorded are the mean values taken from the region of interest for each frame and this results in reading significantly lower values than the ones reported in the literature [21, 27]. In addition, until the flow starts, the temperature values are read between 60-65°C, which is significantly lower than the set mould temperature of 90°C. The reason for this effect is that the polished mould insert surface reflects the cooler temperatures around other sources rather than being a good thermal emitter. Hence, the measured temperature values are therefore a combination of polymer melt and mould surface temperatures.

(2) The filling process is complete at point 2 with considerably higher temperatures due to sustained sonication.

(3) This sustained sonication heats the cavity further, where the highest mean temperature values from the region of interest were recorded as 125.1°C at t = 2.75 s after the filling.

(4) The dramatic change in the rate of cooling from the temperature curve can be attributed to the end of sonication where additional heating energy is no longer provided. This kink in the temperature curve appears to be near t = 3.9 s and a delay of ~100 ms is present between the trigger unit of the thermal camera and the start of sonication. The reason for this effect is attributed to the rate of increase for the trigger signal and digital edge detection mechanism of the thermal camera.

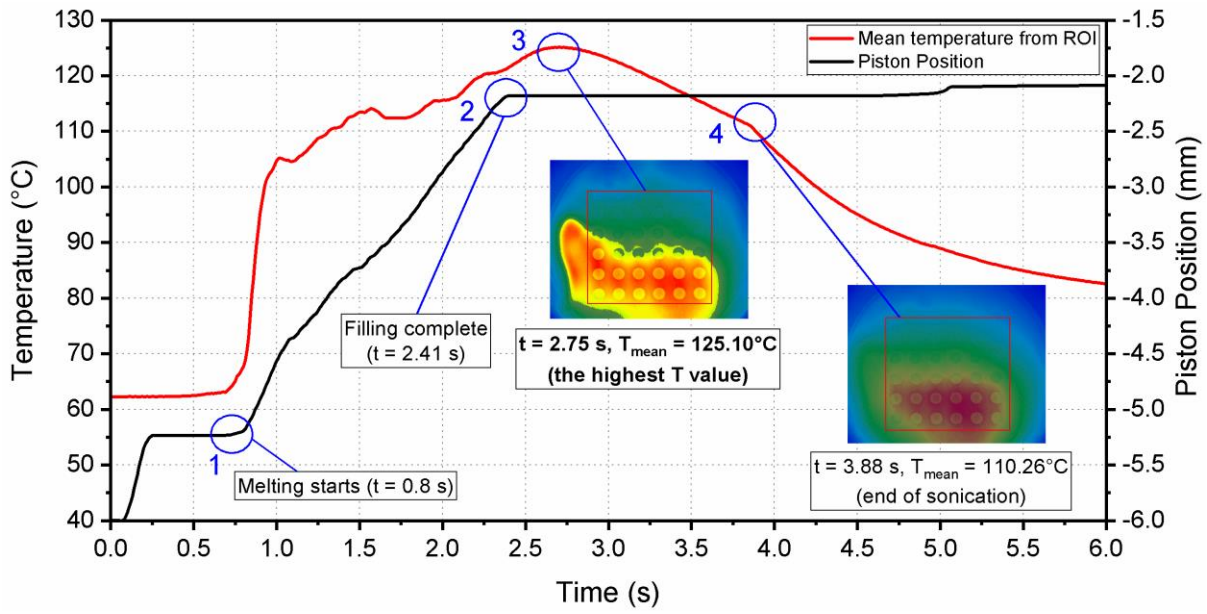

Fig. 10. Graph depicting the mean temperatures recorded from the square region of interest (ROI) that covers the microneedle cavities during the 13th cycle. Important features of the curves are numbered. Point 3 indicates that the hottest temperatures have been witnessed after the filling at t = 2.75 s.

The higher temperature values after the filling process are very likely to be coincident with the highest cavity pressure values as the cavity is completely filled according to the plunger position information. A slight change in plunger position near t = 5 s is insignificant to overall product replication since this movement solely results in flashing effects around the sprue of the part. A decreasing temperature gradient towards the end of the cavity is seen according to the thermal images and data in Fig. 9 and 10. The proximity of the sonotrode to the gate region and attenuation of the ultrasonic waves are the main reasons for this effect.

Fig. 11 shows the maximum temperature values taken from the rectangular region of interest during three consecutive ultrasonic micromoulding experiments. The profiles are significantly different from the conventional micromoulding thermal imaging acquisitions presented in the literature where only a single temperature peak and decay were observed [21, 27]. As shown,

the temperature profiles of ultrasonic micromoulding filling events are characterised by multiple peaks throughout the process. The melting of the material is being carried out progressively and sustained sonication result in wider temperature profiles with sustaining sonication. One of the most significant feature of these results is that the initial peaks, with temperatures as high as 290°C, last only about 100 to 300 ms, which could be advantageous for reducing material degradation. Moreover, these maximum temperature values are highly localised and taken from specific pixels, hence the average temperature of the polymer melt is much lower as indicated previously in Fig.10. This is a significant quantification of one of the advantages of the ultrasonic micromoulding where, the melt is being exposed to higher temperatures for considerably shorter times than in conventional technologies.

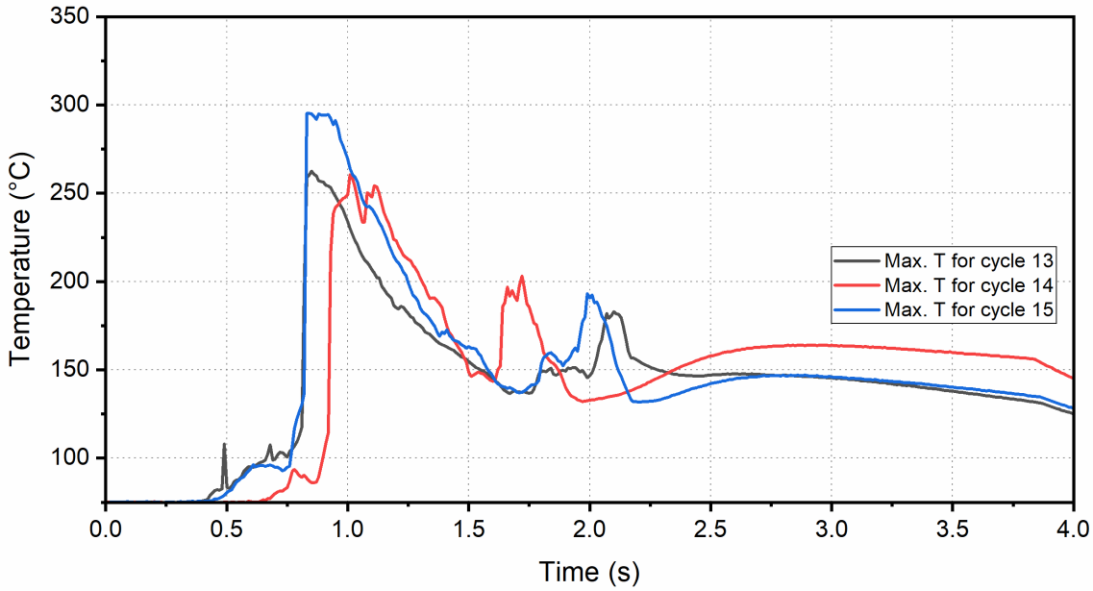

Fig. 11. Maximum temperature profiles taken from three consecutive ultrasonic micromoulding events. The temperature values represent the maximum values read from the ROI that covers the microneedle cavities.

3.3 Cavity pressure measurements

Although cavity pressure measurements have been widely used as a method for condition monitoring purposes in micromoulding [10, 31, 37], no reports were found regarding its usage in ultrasonic processes. An indirect cavity pressure measurement approach has been adopted where the polymer melt is no in direct contact with the transducer surface. This measurement involves a cavity pressure transducer placed at the back of the ejector pin which is at the far end of the cavity (Fig. 12). The reason for implementing this approach is the presumable proximity of a direct cavity pressure sensor to the sonotrode in the mould design and possible damages that can occur to the transducer due to sonication. Moreover, the direct measurement sensor options were also based on piezoelectric techniques and this is very likely to interfere with the applied sonication signal and can cause inaccurate pressure measurements.

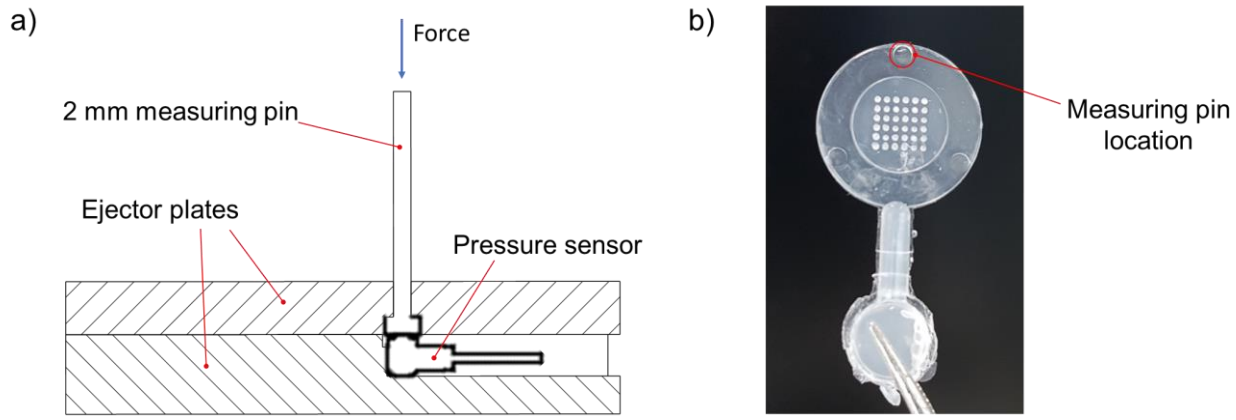

Fig. 12. a) Schematic showing the indirect pressure sensor attachment on the ejector plates; b) an image of one of the ultrasonically moulded parts indicating the location of the measurement pin for cavity pressures.

Fig. 13 shows the cavity pressure profile for the 13th cycle. The plunger position and temperature profiles are also included for more complete interpretation of the data. The main point of interest in this figure is that the peak cavity pressures and mean temperature values

coincide near t = 2.7 s. The cavity pressure peak for this particular cycle is recorded as 87.9 bar. Out of 15 cycles an average cavity pressure peak value of 83.9 bar was recorded (with a standard deviation of 8.01), which is significantly lower than the cavity pressure values taken from conventional micromoulding processes (~200 bar) as presented in the literature [5, 37]. Between t = 2.25 - 4 s slight fluctuations in the cavity pressure data can be observed. These can be attributed to cavitation effect occurring near the sprue and the runner due to sonication, since some bubble formation being observed near the gate in several parts. After the sonication ends at t = 4 s, it can be seen that cavity pressures as high as 20 bar were sustained towards the end of the cycle. The frictional effects and default 500 N force applied by the injection plunger during packing are likely to load the transducer and contribute to this behaviour because of the indirect measurement approach.

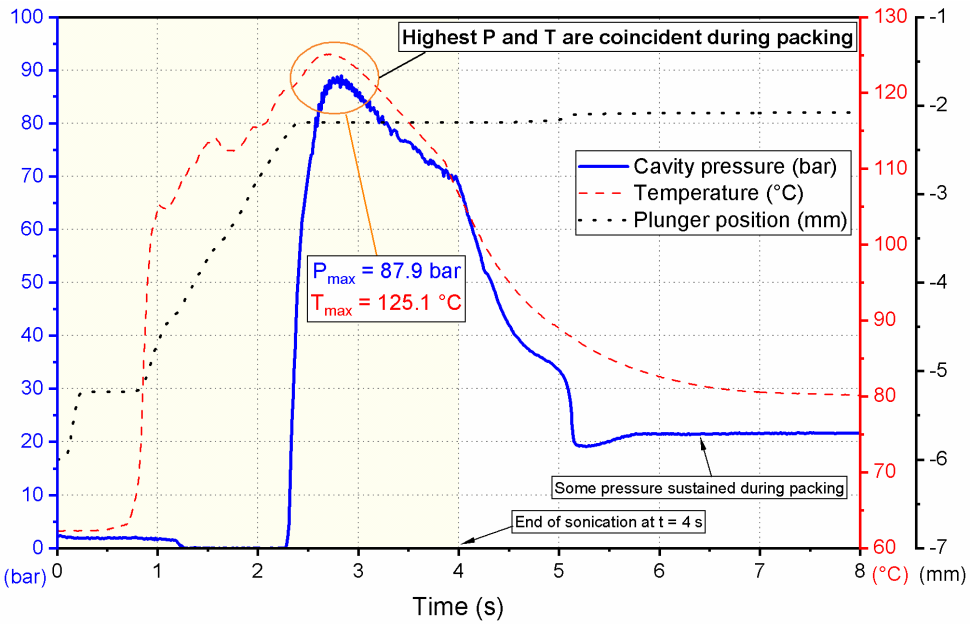

Fig. 13. Graph depicting the cavity pressure behaviour during cycle 13. Plunger position and mean temperature data from ROI are also given.

Fig. 14 depicts the differences between the cavity pressure measurements from different cycles. 3 measurements have been included in the graph that differ from each other significantly for

depicting the variations. It is evident that the peak cavity pressures and their locations are directly in conjunction with the melting process, with some parts being filled quicker owing to with faster emerging flow fronts. Sustained cavity pressures after filling are more prone to variation than the peak cavity pressures exhibiting significantly different pressure values for the three parts presented. This plateau-like behaviour after the main peaks is due to the indirect measurement where minor flashing effects around the ejector pin cause frictional forces and hence the load on the transducer is sustained until the part is ejected at t = 14.5 s.

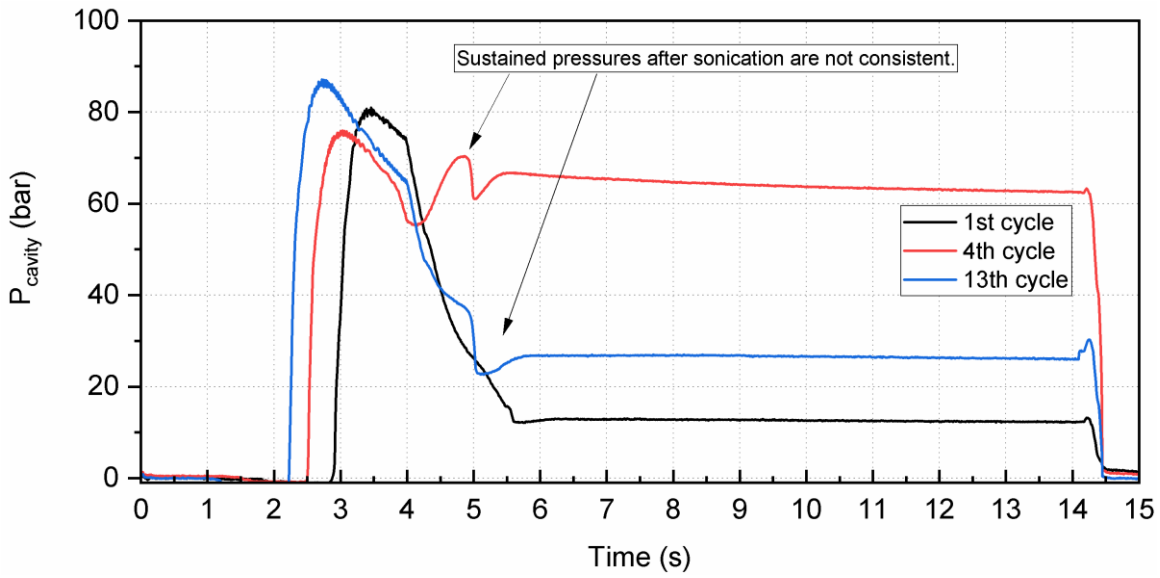

Fig. 14. Cavity pressure profiles for 1st, 4th and 13th cycles.

3.4 Product property measurements

To assess the microreplication capabilities of ultrasonic micromoulding with selected process parameters, manufactured microneedle patches were inspected under a telecentric optical measurement system. The measurement system is based on a 5x telecentric objective lens and a telecentric backlight illuminator. The images and measurements have been acquired using a National Instruments Vision Assistant based LabVIEW script. The system has been calibrated using a 5x calibration target. An example telecentric image of the needles and a scanning electron microscope (SEM – Jeol TM3000) image of a single needle are given in Fig. 15a. It

can be seen that the telecentric images provide good contrast for evaluation of the microneedle height and the SEM image show that the machining marks on the mould walls are replicated completely. From 15 samples, an average needle height of 856 µm with 18 µm of standard deviation has been found. This shows that circa 92% of the microneedle cavity depths have been replicated. Table 4 summarises the results taken from microneedle measurements. The minimum and maximum microneedle heights were found to be 824 and 889 µm, respectively. This large variation between minimum and maximum values is indicative of process variability and can be attributed to differences in the melting behaviour of the PP caused by cycle to cycle temperature and viscosity variations affecting the filling of the cavities.

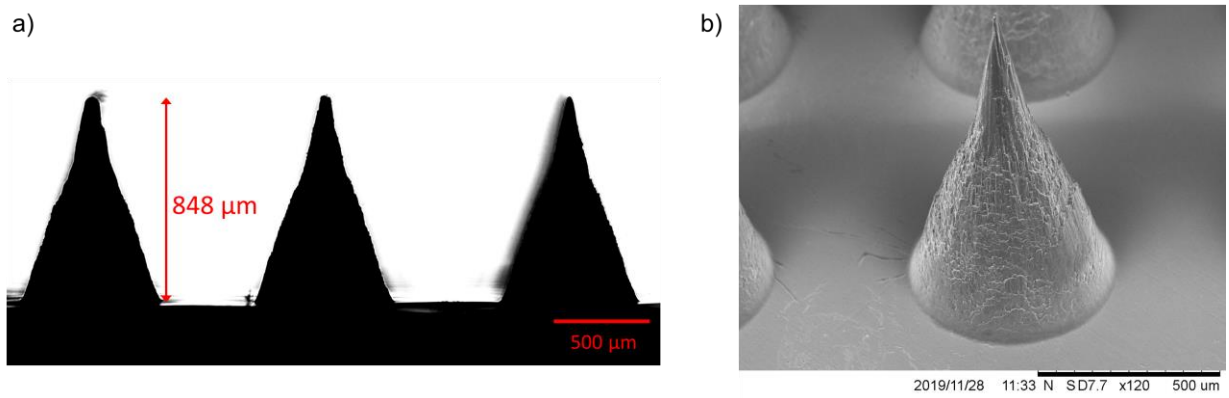

Fig. 15. a) A telecentric optical image of the microneedles; b) an SEM image of a single microneedle taken from one of the patches showing the main features.

Table 4. Microneedle measurement results taken from the parts manufactured in 15 consecutive cycles. Each average needle height represents 36 microneedles on one microneedle part/array.

Average microneedle height (µm)	Standard deviation (µm)	Max. average needle height (µm)	Min. average needle height (µm)
856	18	889	824

3.5 In-line quality assessment using process data

Because of its significance and relevance to the filling process, plunger position was selected for further interrogation and analysis of the process data for in-line quantification of microreplication quality. The analysis was performed as follows:

(i) The part with 'best' microneedle replication quality was determined and plunger position data (x) for this particular sample chosen as the datum.

(ii) Plunger position data of the other 14 samples were subtracted from the 'best' curve defined in (i). Subsequently, the resulting data are defined as Δx curves, which represent the deviations from the 'best' part. Δx curves were then numerically integrated and the deviations for each sample were quantified with a parameter which denotes the deviation of the piston and defined as ∫Δx, representing a generalised proxy for 36 needles on each of the parts.

(iii) A scatter graph with average microneedle height from each cycle vs ∫Δx was plotted for investigating the correlations.

Fig. 16 depicts the relationship between the microneedle height and ∫Δx. The sample with the best replication, and hence with a ∫Δx of zero, is indicated on the leftmost part of the plot. A decreasing trend for average microneedle height was seen with increasing deviation values in the plunger position. A linear fit was chosen to represent the scattered data and R-squared value calculated to quantify the relevance of the fit. An R-squared value of 0.448 has been found for the linear relationship between the microreplication efficiency and piston deviation. This is significant as the plunger position data is readily available from the ultrasonic micromoulding machine interface and does not require an additional sensor technology for in-line monitoring. Moreover, there could be other affects that are influencing the goodness of the correlation such as arrangement of the disc preforms and possible errors that might be caused by the

measurement system. Hence, this channel could be a cost-effective product quality indicator from a micromanufacturing point of view in ultrasonic micromoulding and could predict the microreplication efficiency with decent accuracy.

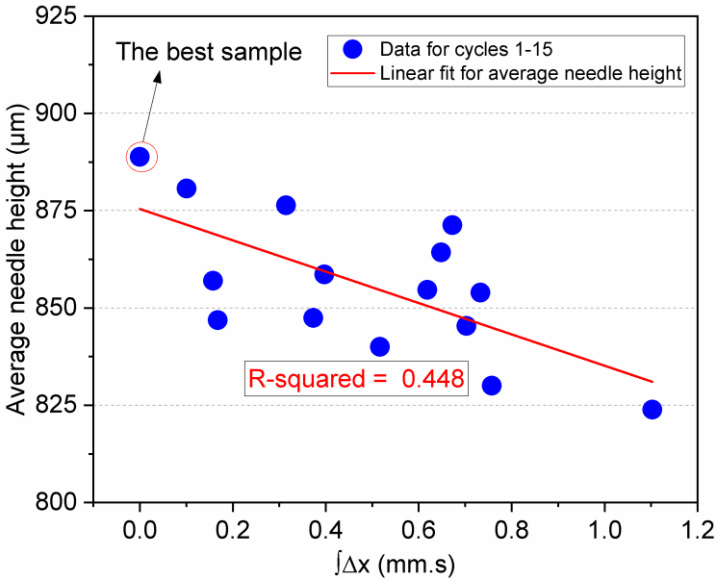

Fig. 16. Scatter plot depicting the relationship between the average needle height and the deviation of the piston (∫Δx) measured from each part and manufacturing cycle. An R-squared value of 0.448 was calculated for the linear fit.

4. Conclusions

This work has presented extensive process monitoring of ultrasonic micromoulding using a variety of sensing capabilities. The study provides an in-depth analysis regarding the dynamics and melting characteristics of ultrasonic micromoulding, which are not reported in the literature so far. The plunger position from machine data has been proved to provide extremely useful information for identifying the melting, filling, and packing phases. Power output and sonication frequency channels are also very beneficial for tuning the process with respect to the process parameters and feedstock shape used. The significance of using as low injection forces as possible is also emphasised since this directly affects the sonication properties of the

ultrasonic stack. Flow visualisation using thermal imaging was found to be a powerful technique for quantifying the temperature evolution during ultrasonic micromoulding. The temperature profiles proved to be very different from conventional micromoulding processes where the highest temperatures witnessed after the filling. The highest cavity pressures also accompanied and coincided with the highest temperatures and this proves that ultrasonic micromoulding could be a viable alternative to conventional technologies for better replication of micro and nano features.

Another important outcome of the work is the significance of plunger position data for in-line monitoring purposes for micro-scaled products. The plunger position was proved to be a cost-effective process and product quality indicator when manufacturing microneedle devices in a pilot production run. Key geometrical dimensions/features of the products can be monitored indirectly due to their linear relationships with the deviation in plunger position data with decent accuracy. Furthermore, cost-effectiveness of a quality-assurance procedure usually outweighs the accuracy of the method when additional amount of data from cycles are included. Thus, the plunger position data will be extremely useful for potential micro-manufacturing scenarios and shown to be the best machine variable to indicate filling quality in this work.

Further investigations on ultrasonic micromoulding process are required for improving its repeatability and reliability. For instance, a variotherm approach involving a rapid heating and cooling of the mould can be implemented for achieving better replication and for mitigating the cycle to cycle variation with minimal impact on the cycle times. However, this could be a challenging task depending on the part design that affects the moulding behaviour and process parameters almost entirely. Nevertheless, this research signifies the importance of in-line condition monitoring for this new and unique manufacturing technique and provides a datum for characterising the ultrasonic micromoulding process. The monitoring tools and approaches

discussed here will allow identifying the sources of variations in the process for making this technology more reliable.

Acknowledgement

This research work was undertaken in the context of MICROMAN project ("Process Fingerprint for Zero-defect Net-shape MICROMANufacturing", http://www.microman.mek.dtu.dk/). MICROMAN is a European Training Network supported by Horizon 2020, the EU Framework Programme for Research and Innovation (Project ID: 674801). This research has also received funding and support from two other Horizon 2020 projects: HIMALAIA (Grant agreement No. 766871) and Laser4Fun (GA no. 675063).

REFERENCES

[1] B. R. Whiteside, M. T. Martyn, P. D. Coates, P. S. Allan, P. R. Hornsby, and G. Greenway, "Micromoulding: Process characteristics and product properties," *Plastics, Rubber and Composites,* Article vol. 32, no. 6, pp. 231-239, 2003, doi: 10.1179/146580103225002650.

[2] F. Baruffi *et al.*, "Correlating nano-scale surface replication accuracy and cavity temperature in micro-injection moulding using in-line process control and high-speed thermal imaging," *Journal of Manufacturing Processes,* vol. 47, pp. 367-381, 2019/11/01/ 2019, doi: https://doi.org/10.1016/j.jmapro.2019.08.017.

[3] J. M. Romano, M. Gulcur, A. Garcia-Giron, E. Martinez-Solanas, B. R. Whiteside, and S. S. Dimov, "Mechanical durability of hydrophobic surfaces fabricated by injection moulding of laser-induced textures," *Applied Surface Science,* Article vol. 476, pp. 850-860, 2019, doi: 10.1016/j.apsusc.2019.01.162.

[4] J.-M. Romano, A. Garcia-Giron, P. Penchev, M. Gulcur, B. R. Whiteside, and S. Dimov, "Lotus-Leaf Inspired Surfaces: Hydrophobicity Evolution of Replicas Due to Mechanical Cleaning and Mold Wear," *Journal of Micro and Nano-Manufacturing,* vol. 8, no. 1, 2020, doi: 10.1115/1.4046097.

[5] N. Zhang, H. Zhang, C. Stallard, F. Fang, and M. D. Gilchrist, "Replication integrity of micro features using variotherm and vacuum assisted microinjection moulding," *CIRP Journal of Manufacturing Science and Technology,* vol. 23, pp. 20-38, 2018/11/01/ 2018, doi: https://doi.org/10.1016/j.cirpj.2018.10.002.

[6] G. Tosello, A. Gava, H. N. Hansen, and G. Lucchetta, "Study of process parameters effect on the filling phase of micro-injection moulding using weld lines as flow markers," *The International Journal of Advanced Manufacturing Technology,* vol. 47, no. 1, pp. 81-97, 2010/03/01 2010, doi: 10.1007/s00170-009-2100-1.

[7] B. R. Whiteside, E. C. Brown, Y. Ono, C. K. Jen, and P. D. Coates, "Real-time ultrasonic diagnosis of polymer degradation and filling incompleteness in micromoulding," *Plastics, Rubber and Composites,* Article vol. 34, no. 9, pp. 387-392, 2005, doi: 10.1179/174328905X71977.

[8] N. Zhang and M. D. Gilchrist, "Characterization of thermo-rheological behavior of polymer melts during the micro injection moulding process," *Polymer Testing,* vol. 31, no. 6, pp. 748-758, 2012/09/01/ 2012, doi: https://doi.org/10.1016/j.polymertesting.2012.04.012.

[9] U. Heredia-Rivera, I. Ferrer, and E. Vázquez, "Ultrasonic Molding Technology: Recent Advances and Potential Applications in the Medical Industry," *Polymers,* vol. 11, no. 4, 2019, doi: 10.3390/polym11040667.

[10] B. R. Whiteside, R. Spares, K. Howell, M. T. Martyn, and P. D. Coates, "Micromoulding: Extreme process monitoring and inline product assessment," *Plastics, Rubber and Composites,* Article vol. 34, no. 9, pp. 380-386, 2005, doi: 10.1179/174328905X72011.

[11] H. V. Fairbanks, "Applying ultrasonics to the moulding of plastic powders," *Ultrasonics,* Article vol. 12, no. 1, pp. 22-24, 1974, doi: 10.1016/0041-624X(74)90082-1.

[12] W. Michaeli, A. Spennemann, and R. Gärtner, "New plastification concepts for micro injection moulding," *Microsystem Technologies,* Article vol. 8, no. 1, pp. 55-57, 2002, doi: 10.1007/s00542-001-0143-9.

[13] W. Michaeli, T. Kamps, and C. Hopmann, "Manufacturing of polymer micro parts by ultrasonic plasticization and direct injection," *Microsystem Technologies,* Article vol. 17, no. 2, pp. 243-249, 2011, doi: 10.1007/s00542-011-1236-8.
[14] M. Janer, X. Plantà, and D. Riera, "Ultrasonic moulding: Current state of the technology," *Ultrasonics,* vol. 102, p. 106038, 2020/03/01/ 2020, doi: https://doi.org/10.1016/j.ultras.2019.106038.
[15] E. Colavizza, F. Puliga, and E. Escudero, "Sonoplast. "New process and machinery for microparts molding based on ultrasound excitation"," in *Annual Technical Conference - ANTEC, Conference Proceedings*, 2010, vol. 1, pp. 15-21. [Online]. Available: https://www.scopus.com/inward/record.uri?eid=2-s2.0-77956701100&partnerID=40&md5=a7535ad63ab98dfc17c00612d3667251
[16] K. Zeng *et al.*, "Process and properties of micro-ultrasonic powder molding with polypropylene," *The International Journal of Advanced Manufacturing Technology,* vol. 70, no. 1, pp. 515-522, 2014/01/01 2014, doi: 10.1007/s00170-013-5300-7.
[17] M. Sacristán, X. Plantá, M. Morell, and J. Puiggalí, "Effects of ultrasonic vibration on the micro-molding processing of polylactide," *Ultrasonics Sonochemistry,* Article vol. 21, no. 1, pp. 376-386, 2014, doi: 10.1016/j.ultsonch.2013.07.007.
[18] T. Dorf, I. Ferrer, and J. Ciurana, "Characterizing ultrasonic micro-molding process of polyetheretherketone (PEEK)," *International Polymer Processing,* Article vol. 33, no. 4, pp. 442-452, 2018, doi: 10.3139/217.3428.
[19] B. Jiang, H. Peng, W. Wu, Y. Jia, and Y. Zhang, "Numerical simulation and experimental investigation of the viscoelastic heating mechanism in ultrasonic plasticizing of amorphous polymers for micro injection molding," *Polymers,* Article vol. 8, no. 5, 2016, Art no. 199, doi: 10.3390/polym8050199.
[20] B. Whiteside, M. Babenko, C. Tuinea-Bobe, E. Brown, and P. Coates, "Ultrasonic injection moulding: A study of thermal behaviour and nanofeature replication," in *Proceedings of the 16th International Conference of the European Society for Precision Engineering and Nanotechnology, EUSPEN 2016*, 2016. [Online]. Available: https://www.scopus.com/inward/record.uri?eid=2-s2.0-84984619801&partnerID=40&md5=cf069c46878f156d890ce3c551350c5d
[21] D. Masato, M. Babenko, B. Shriky, T. Gough, G. Lucchetta, and B. Whiteside, "Comparison of crystallization characteristics and mechanical properties of polypropylene processed by ultrasound and conventional micro-injection molding," *The International Journal of Advanced Manufacturing Technology,* vol. 99, no. 1, pp. 113-125, 2018/10/01 2018, doi: 10.1007/s00170-018-2493-9.
[22] W. Wu, H. Peng, Y. Jia, and B. Jiang, "Characteristics and mechanisms of polymer interfacial friction heating in ultrasonic plasticization for micro injection molding," *Microsystem Technologies,* Article vol. 23, no. 5, pp. 1385-1392, 2017, doi: 10.1007/s00542-016-2877-4.
[23] M. Gulcur, B. R. Whiteside, K. Nair, M. Babenko, and P. D. Coates, "Ultrasonic injection moulding of polypropylene and thermal visualisation of the process using a bespoke injection mould tool," in *European Society for Precision Engineering and Nanotechnology, Conference Proceedings - 18th International Conference and Exhibition, EUSPEN 2018*, 2018, pp. 243-244. [Online]. Available: https://www.scopus.com/inward/record.uri?eid=2-s2.0-85054508180&partnerID=40&md5=1685626ffd5922ac1817c7c325fc1dae
[24] P. Penchev, S. Dimov, D. Bhaduri, S. L. Soo, and B. Crickboom, "Generic software tool for counteracting the dynamics effects of optical beam delivery systems," *Proceedings of the Institution of Mechanical Engineers, Part B: Journal of*

Engineering Manufacture, vol. 231, no. 1, pp. 48-64, 2017/01/01 2015, doi: 10.1177/0954405414565379.

[25] J. M. Fischer, *Handbook of Molded Part Shrinkage and Warpage* (Handbook of Molded Part Shrinkage and Warpage). 2003, pp. 1-252.

[26] B. R. Whiteside *et al.*, "Optical imaging metrology for micromoulding cavity flows and products," *Plastics, Rubber and Composites,* Conference Paper vol. 37, no. 2-4, pp. 57-66, 2008, doi: 10.1179/174328908X283384.

[27] M. Babenko, J. Sweeney, P. Petkov, F. Lacan, S. Bigot, and B. Whiteside, "Evaluation of heat transfer at the cavity-polymer interface in microinjection moulding based on experimental and simulation study," *Applied Thermal Engineering,* Article vol. 130, pp. 865-876, 2018, doi: 10.1016/j.applthermaleng.2017.11.022.

[28] P. Negre, J. Grabalosa, I. Ferrer, J. Ciurana, A. Elías-Zúñiga, and F. Rivillas, "Study of the Ultrasonic Molding Process Parameters for Manufacturing Polypropylene Parts," *Procedia Engineering,* vol. 132, pp. 7-14, 2015/01/01/ 2015, doi: https://doi.org/10.1016/j.proeng.2015.12.460.

[29] W. Michaeli and D. Opfermann, *Ultrasonic plasticising for micro injection moulding*. Woodhead Publishing Limited, 2006, pp. 345-348.

[30] X. Sánchez-Sánchez, M. Hernández-Avila, L. E. Elizalde, O. Martínez, I. Ferrer, and A. Elías-Zuñiga, "Micro injection molding processing of UHMWPE using ultrasonic vibration energy," *Materials and Design,* Article vol. 132, pp. 1-12, 2017, doi: 10.1016/j.matdes.2017.06.055.

[31] B. R. Whiteside, M. T. Martyn, P. D. Coates, G. Greenway, P. Allen, and P. Hornsby, "Micromoulding: Process measurements, product morphology and properties," *Plastics, Rubber and Composites,* Conference Paper vol. 33, no. 1, pp. 11-17, 2004, doi: 10.1179/146580104225018346.

[32] M. Worgull, *Hot Embossing* (Hot Embossing). 2009.

[33] R. Spares, B. R. Whiteside, and P. D. Coates, "High speed thermal imaging of micromoulding," in *Annual Technical Conference - ANTEC, Conference Proceedings*, 2009, vol. 5, pp. 2570-2573. [Online]. Available: https://www.scopus.com/inward/record.uri?eid=2-s2.0-70450008441&partnerID=40&md5=7d3b816d632aa6771871acdf24515e71

[34] R. Spares, B. R. Whiteside, and P. D. Coates, "High speed thermal imaging of complex micromoulding flows," in *Annual Technical Conference - ANTEC, Conference Proceedings*, 2013, vol. 2, pp. 1556-1559. [Online]. Available: https://www.scopus.com/inward/record.uri?eid=2-s2.0-84903527348&partnerID=40&md5=4adf44ff511fbe5dc091d01097c44718

[35] F. Baruffi, M. Calaon, and G. Tosello, "Micro-Injection Moulding In-Line Quality Assurance Based on Product and Process Fingerprints," *Micromachines,* vol. 9, no. 6, 2018, doi: 10.3390/mi9060293.

[36] E. C. Brown, L. Mulvaney-Johnson, and P. D. Coates, "Ultrasonic measurement of residual wall thickness during gas assisted injection molding," *Polymer Engineering and Science,* Article vol. 47, no. 11, pp. 1730-1739, 2007, doi: 10.1002/pen.20832.

[37] C. A. Griffiths, S. S. Dimov, S. Scholz, H. Hirshy, and G. Tosello, "Process factors influence on cavity pressure behavior in microinjection moulding," *Journal of Manufacturing Science and Engineering, Transactions of the ASME,* Article vol. 133, no. 3, 2011, Art no. 031007, doi: 10.1115/1.4003953.